

# Demonstration of reconfigurable electro-optical logic with silicon photonic integrated circuits

Ciyuan Qiu,<sup>1</sup> Xin Ye,<sup>1</sup> Richard Soref,<sup>2</sup> Lin Yang,<sup>3</sup> and Qianfan Xu<sup>1,\*</sup>

<sup>1</sup>Department of Electrical and Computer Engineering, Rice University, Houston, Texas 77005, USA

<sup>2</sup>Department of Physics, University of Massachusetts, Boston, Massachusetts 02125, USA

<sup>3</sup>Institute of Semiconductors, Chinese Academy of Sciences, P.O. Box 912, Beijing 100083, China

\*Corresponding author: qianfan@rice.edu

Received July 5, 2012; revised August 20, 2012; accepted August 21, 2012;

posted August 22, 2012 (Doc. ID 171932); published September 18, 2012

We demonstrate a scalable and reconfigurable optical directed-logic architecture consisting of a regular array of integrated optical switches based on microring resonators. The switches are controlled by electrical input logic signals through embedded p-i-n junctions. The circuit can be reconfigured to perform any combinational logic operation by thermally tuning the operation modes of the switches. Here we show experimentally a directed logic circuit based on a  $2 \times 2$  array of switches. The circuit is reconfigured to perform arbitrary two-input logic functions. © 2012 Optical Society of America

OCIS codes: 130.0130, 230.3750, 230.5750.

We have recently proposed a new (to our knowledge) reconfigurable and cellular electro-optical (EO) logic architecture [1] that is well suited for complementary metal-oxide-semiconductor (CMOS)-compatible silicon photonics. The idea is to create large-scale-integrated (LSI) reconfigurable optical logic fabrics as an optical equivalent of a field-programmable gate array (FPGA). The design is based on the directed-logic paradigm that minimizes the latency in calculating a complicated logic function [2,3] by taking advantage of the fast and low-loss propagation of light.

The logic circuit is formed by a uniform two-dimensional array of reconfigurable on-off EO switches connected by parallel optical waveguides. The state of each switch is controlled by an electrical input logic signal. In this circuit, all the switches flip simultaneously, and their switching times do not accumulate—in contrast to electronic transistor logic circuits, wherein gate delays are cascaded to introduce a relatively large latency. A combinational logic function is calculated when its truth table is mapped onto the operation modes of the switches. The low latency and fast reconfigurability of the logic circuit make it useful for many applications. One example is to quickly look up a routing table in a packet-switched optical interconnection network, where the routing table can be dynamically updated [4].

In this Letter, we present a proof-of-concept demonstration using a multispectral implementation of the electro-optic logic circuit as discussed in [1]. With a  $2 \times 2$  array of reconfigurable switches, this logic circuit can perform arbitrary two-input logic functions.

The basic building block of the logic circuit is a reconfigurable EO switch based on silicon microring resonators [5–12]. Each switch has an embedded p-i-n junction for logic input and a microheater for reconfiguration. This type of switch has small size [7], fast switching speed [8], low power consumption [9,10], and the capability of large-scale integration [11]. Each switch can be reconfigured by thermal tuning [13,14] to one of three operation modes, as will be shown in Fig. 1.

The EO logic circuits are fabricated in a CMOS photonics foundry at the Institute of Microelectronics of

Singapore [15]. The fabrication starts on a silicon-on-insulator (SOI) wafer with 220 nm thick top silicon and 3  $\mu\text{m}$  thick buried oxide. Rib waveguides with a 500 nm width, 220 nm height, and 50 nm slab thickness are used to construct the photonic circuit. The switches are based on microring resonators with diameters of  $\sim 10 \mu\text{m}$  that are side-coupled to straight waveguides. A deep-UV lithography process is used to define the device pattern, which is etched into the silicon layer by inductively coupled plasma etching. Following the etching, the p-i-n junctions are formed across the ring, as illustrated in Fig. 1(a), by patterned ion implantations. A 1.6  $\mu\text{m}$  thick  $\text{SiO}_2$  layer is then deposited onto the wafer using plasma-enhanced chemical vapor deposition (PECVD). A 150 nm thick patterned titanium nitride (TiN) layer is sputtered on the oxide to form the microheaters. Another 500 nm thick  $\text{SiO}_2$  layer is deposited by PECVD. Finally, vias are opened on the implanted areas and the microheaters, and a 1.5  $\mu\text{m}$  thick aluminum layer is sputtered and etched to form the electric connections. After the fabrication process, the contact pads on the chip are wire-bonded to a

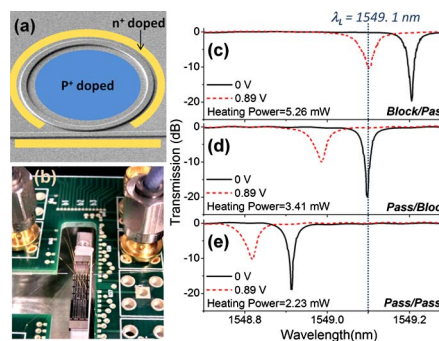


Fig. 1. (Color online) (a) SEM picture of the microring resonator after etching. The false color shows the implanted areas. (b) Device mounted on a stage and wire-bonded to a PCB board. (c) The transmission spectra of a switch in *block/pass* mode for light at working wavelength  $\lambda_L$ . The red dashed curve and the black solid curve are the spectra when the applied modulation signal is 0.89 and 0 V, respectively. (d) The transmission spectra of a switch in *pass/block* mode. (e) The transmission spectra of a switch in *pass/pass* mode.

custom-made interface board as shown in Fig. 1(b). The microheaters are controlled by a computer through digital-to-analog converters. The p-i-n junctions of the switches are wire-bonded to SMA connectors with 50 Ohm terminal resistors for impedance matching.

The transmission spectra of the TE mode of a switch are measured with a tunable laser. Sharp resonance dips can be clearly seen in Fig. 1(c). When free carriers are injected into the p-i-n junction with a forward bias voltage of 0.89 V (logic “1”), the resonance blueshifts. The depth of the resonance decreases due to the free-carrier absorption effect [16]. At the input laser wavelength of  $\lambda_L = 1549.1$  nm, the optical transmission is low when the bias voltage is high (logic “1”) and the transmission is high when the bias voltage is zero or negative (logic “0”). We call this operation mode of the switch the *block/pass* mode. In this mode, the quality factor is 41,000 for the *pass* state and 31,000 for the *block* state. As the working wavelength is fixed at 1549.1 nm, the operation mode can be reconfigured to be the *pass/block* mode or the *pass/pass* mode, as shown in the Figs. 1(d) and 1(e) respectively, by changing the heating power on the integrated microheater. In the *pass/block* mode, the switch has a 20 dB extinction ratio, while in the *block/pass* mode, the switch has a 10 dB extinction ratio. The thermo-optic reconfiguration time is measured to be  $<35$   $\mu$ s. The insertion loss of each switch is  $\sim 0.15$  dB, which can be further reduced with a larger tuning range.

The structure of the reconfigurable logic circuit for arbitrary two-input logic functions is illustrated in Fig. 2. Each of the two optical waveguides marked by the horizontal black lines passes through two optical switches. Represented by vertical black lines are an optical input waveguide and an optical output waveguide. The red lines represent the electrical logic input signals (operands *A* and *B*) applied on the optical switches. Each operand controls two switches in different waveguides simultaneously. Since light can pass a waveguide (corresponding to an output logic “1”) when both switches are in the *pass* state, the output of the waveguide carries a product function (logic AND operation) depending on the operation mode of the two switches. For example, if the switch controlled by *A* is in the *pass/block* mode and the switch controlled by *B* is in the *block/pass* mode, the optical output carries the product  $AB$ . If the switch controlled by *A* is in the *pass/block* mode and the other switch is in the *pass/pass* mode, the optical output is *A*.

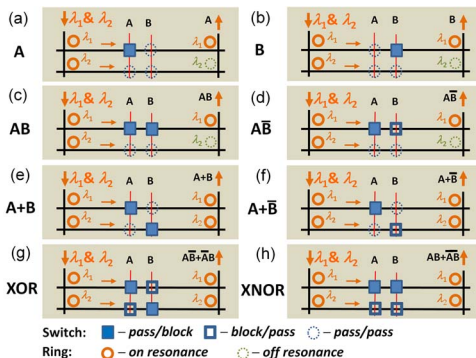


Fig. 2. (Color online) Circuit diagrams of the EO logic circuits for different two-input logic functions.

This way, any product between the two operands, their inversion, and “1” can be obtained at the end of each horizontal waveguide by reconfiguring the operation modes of the two switches in this waveguide.

Any two-input combinational logic function can be expressed as a sum (logic OR operation) of two products. The sum is performed by incoherently adding the output optical signals from the two waveguides that calculate the two products. In our design, the microrings in the same horizontal waveguide are designed to have the same diameter, while rings at different horizontal waveguides will have slightly different diameters. The two waveguides can then operate at different wavelengths to avoid optical interference. As the circuit diagrams in Fig. 2 show, two lasers with different wavelengths ( $\lambda_1$  and  $\lambda_2$ ) are sent into the input waveguide (the vertical line on the left). They are separated and dropped into the two logic (horizontal) waveguides by the “passive” microring resonators at the crossing points. At the output side of a logic waveguide, the light is redirected to an output (vertical) waveguide if the product calculated by this waveguide is part of the logic function to be calculated. This is done by thermally tuning the output microring resonator at the crossing point to be on resonance (represented by the orange circles) with the light in the waveguide. Otherwise, the output microring resonator will be tuned away from the laser wavelength (represented by the green dashed circles), and light in the horizontal waveguide will not be collected by the vertical waveguide [1].

Light from the output waveguide is coupled to a fiber and sent to a broadband photodetector that absorbs photons at all source wavelengths and creates a photocurrent that sums the optical outputs from the horizontal waveguides that couple to the output waveguide. The output logic signal will be defined as “1” if any one of the horizontal waveguides has a high-level output. This performs the sum (logic OR) function of the products calculated by the coupled horizontal waveguides.

Microheaters are integrated with the add/drop microring filters at the crossing points between the horizontal and vertical waveguides for thermal tuning, but no p-i-n junctions are embedded in these rings. At the crossing points between the waveguides, the width of the waveguide is extended to be 1  $\mu$ m in order to reduce the optical loss [17]. Inverse tapers with 180 nm wide tips are integrated for input and output terminals of the waveguides to enhance the coupling between the waveguides and tapered lens fibers [3]. The coupling loss is  $\sim 4.5$  dB per facet.

We have realized all the sixteen possible two-input logic functions just by thermally reconfiguring the operation modes of the switches and tuning the output add/drop microring resonators. Due to space limitations, we show here the results for eight representative functions. In all the demonstrations, the laser wavelengths are fixed at 1549.10 and 1559.16 nm, and the two logic signals are also fixed with a bit rate of 0.526 Gb/s, a high level of 0.8 V (logic “1”), and a low level of  $-1.2$  V (logic “0”). The total consumed RF power is about 8  $\mu$ W, and the total heating power used in the demonstration ranges from 24 to 26 mW for the different logic functions. The output powers of the two lasers are both 5 dBm.

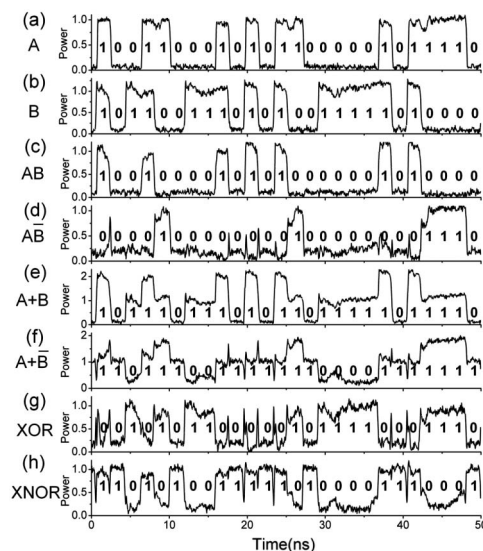


Fig. 3. Waveforms of the output optical signal from the two-input logic circuits shown in Fig. 2. The two input electrical control signals are non-return-to-zero (NRZ)  $2^7 - 1$  pseudorandom bit sequence signals at 526 MHz. They are both set to be  $2V_{pp}$  between  $-1.2$  V and  $0.8$  V.

They are combined with a 50/50 fiber coupler and then coupled into the circuit through a tapered lens fiber.

The circuit diagrams in Figs. 2(a)–2(h) show the operation modes of the switches and the output rings when each logic function is performed. Figures 3(a)–3(h) show the waveform of the output optical signal. In Figs. 3(a) and 3(b), the output logic signals are same as inputs  $A$  and  $B$ , respectively. In Figs. 3(a)–3(d), only light from the top waveguide is coupled to the output waveguide, because the logic function has only one product. In Figs. 3(e) and 3(f), there are two high levels corresponding to the case when one waveguide passes light and when both waveguides pass light, respectively. Both will be judged as logic “1”. In Figs. 3(d) and 3(f)–3(h), there are some positive spikes between two consecutive “0”s and some negative spikes between two consecutive “1”s. This happens when one switch is turning off while the other switch is turning on. The height of the spikes depends on the timing of the rising and falling edges of the two switches. Since the spikes are only at the bit transition regions, they do not affect correct decoding of the bits.

In conclusion, we demonstrated a scalable and reconfigurable optical logic architecture that is based on a

regular array of integrated optical switches. We show a small-scale circuit that can be reconfigured to perform arbitrary two-input combinational logic functions. The demonstrated speed of  $\sim 0.5$  Gb/s is currently limited by the wire-bonding approach. Higher speed can be expected by improving the probing method, by using pre-emphasized driving signals [18], or by using reverse-biased p-n junctions [9,10] for faster switching.

This work was supported by the Air Force Office of Scientific Research (AFOSR grants FA9550-12-1-0261 and FA9550-10-1-0417).

## References

1. Q. Xu and R. Soref, *Opt. Express* **19**, 5244 (2011).
2. J. Hardy and J. Shamir, *Opt. Express* **15**, 150 (2007).
3. L. Zhang, J. Ding, Y. Tian, R. Ji, L. Yang, H. Chen, P. Zhou, Y. Lu, W. Zhu, and R. Min, *Opt. Express* **20**, 11605 (2012).
4. Q. Xu and R. Soref, in *Proceedings of the 8th IEEE International Conference on Group IV Photonics* (IEEE, 2011), pp. 39–41.
5. Q. Xu, B. Schmidt, S. Pradhan, and M. Lipson, *Nature* **435**, 325 (2005).
6. L. Chen, K. Preston, S. Manipatruni, and M. Lipson, *Opt. Express* **17**, 15248 (2009).
7. Q. Xu, D. Fattal, and R. G. Beausoleil, *Opt. Express* **16**, 4309 (2008).
8. Y. Hu, X. Xiao, H. Xu, X. Li, K. Xiong, Z. Li, T. Chu, Y. Yu, and J. Yu, *Opt. Express* **20**, 15079 (2012).
9. P. Dong, S. Liao, D. Feng, H. Liang, D. Zheng, R. Shafiiha, C.-C. Kung, W. Qian, G. Li, X. Zheng, A. V. Krishnamoorthy, and M. Asghari, *Opt. Express* **17**, 22484 (2009).
10. M. R. Watts, W. A. Zortman, D. C. Trotter, R. W. Young, and A. L. Lentine, *Opt. Express* **19**, 21989 (2011).
11. A. Biberman and K. Bergman, *Rep. Prog. Phys.* **75**, 046402 (2012).
12. P. Dong, R. Shafiiha, S. Liao, H. Liang, N. Feng, D. Feng, G. Li, X. Zheng, A. V. Krishnamoorthy, and M. Asghari, *Opt. Express* **18**, 10941 (2010).
13. C. Qiu, J. Shu, Z. Li, X. Zhang, and Q. Xu, *Opt. Express* **19**, 5143 (2011).
14. L. Fan, J. Wang, L. T. Varghese, H. Shen, B. Niu, Y. Xuan, A. M. Weiner, and M. Qi, *Science* **335**, 447 (2012).
15. X. Luo, J. Song, S. Feng, A. W. Poon, T. Liow, M. Yu, G. Lo, and D. Kwong, *IEEE Photon. Technol. Lett.* **24**, 821 (2012).
16. R. A. Soref and B. R. Bennett, *IEEE J. Quantum Electron.* **23**, 123 (1987).
17. F. Xu and A. W. Poon, *Opt. Express* **16**, 8649 (2008).
18. Q. Xu, S. Manipatruni, B. Schmidt, J. Shakya, and M. Lipson, *Opt. Express* **15**, 430 (2007).